proceedings

Proceeding Paper

Impact of Hole Transport Layers in Inorganic Lead-Free B-γ-$CsSnI_3$ Perovskite Solar Cells: A Numerical Analysis †

Adnan Hosen [1,*], Sabrina Rahman [1], Maroua Brella [2] and Sheikh Rashel Al Ahmed [1,*]

[1] Department of Electrical, Electronic and Communication Engineering, Pabna University of Science and Technology, Pabna 6600, Bangladesh; srmithila@gmail.com
[2] Laboratoire de Rayonnement et Plasmas et Physique des Surfaces (LRPPS), Université Kasdi Merbah, Ouargla 30000, Algeria; brellamar@gmail.com
* Correspondence: adnan_hosen@yahoo.com (A.H.); rashel@pust.ac.bd (S.R.A.A)
† Presented at the 1st International Electronic Conference on Processes: Processes System Innovation, 17–31 May 2022; Available online: https://ecp2022.sciforum.net.

Abstract: Tin-based halide perovskite compounds have attracted enormous interest as effective replacement to the conventional lead halide perovskite solar cells (PCSs). However, getting high efficiency for tin-based perovskite solar cells is still challenging. Herein, we introduce copper sulfide (CuS) as hole transport material (HTM) in lead free tin-based B-γ-$CsSnI_3$ PSCs to enhance the photovoltaic (PV) performances. The lead free tin-based $CsSnI_3$ perovskite solar cell structure consisting of CuS/$CsSnI_3$/TiO_2/ITO has been modeled and investigated the output characteristics by using the one dimensional solar cell capacitance simulator (SCAPS-1D). The CuS hole transport layer (HTL) with proper band arrangement may notably minimize the recombination of charge carrier at the back side of the perovskite absorber. Density functional theory (DFT) -extracted physical parameters including band gap and absorption spectrum of CuS are used in the SCAPS-1D program to analyze the characteristics of the proposed PV device. The PV performance parameters of the proposed device are numerically evaluated by varying the absorber thickness and doping concentration. In this work, the variation of the functional temperature on the cell outputs is also studied. Furthermore, different HTMs are employed to investigate the PV characteristics of the proposed $CsSnI_3$ PSC. The power conversion efficiency (PCE) of ~29% is achieved with open circuit voltage (V_{oc}) of 0.99 V, fill factor of ~87%, and short circuit current density (J_{sc}) of 33.5 mA/cm^2 for the optimized device. This works addresses a proper guideline and introduces a convenient approach to design and fabricate highly efficient, inexpensive, and stable lead free tin-based perovskite solar cells.

Keywords: perovskite; B-γ-$CsSnI_3$; HTL; CuS; DFT; SCAPS-1D

Citation: Hosen, A.; Rahman, S.; Brella, M.; Ahmed, S.R.A. Impact of Hole Transport Layers in Inorganic Lead-Free B-γ-$CsSnI_3$ Perovskite Solar Cells: A Numerical Analysis. *Proceedings* **2022**, *69*, x. https://doi.org/10.3390/xxxxx

Academic Editor(s):

Published: date

1. Introduction

The PSCs have fascinated great consideration as encouraging PV technology due to admirable properties associated with excellent PCE and low fabrication cost. This new class of PV technology has recently received enormous interest owing to the emerging conversion efficiency of ~25% [1,2]. However, the rapid growth and commercialization of PSCs are impeded because of toxicity present in most commonly developed lead-based perovskite solar cells [3]. In this context, various attempts have been made in search of suitable alternative for the lead-based perovskites [4–6]. Among different perovskite materials, the inorganic cesium tin triiodide ($CsSnI_3$) may be considered as one of the potential candidates [7]. $CsSnI_3$ exhibits suitable optoelectronic properties including an ideal range of energy gap of ~1.3 eV, absorption coefficient (10^4 cm^{-1}), high charge-carrier mobilities (above 500 cm^2 V^{-1} s^{-1}) and low exciton binding energy (~18 meV) [7,8]. In the previous work, an efficiency of 0.9% is reported with the architecture of indium tin oxide/$CsSnI_3$/Au/Ti in 2012 [9]. An earlier research evaluated a maximum power conversion efficiency (PCE) of 5.03% for $CsSnI_3$ PVQD-based solar cells [10]. Recently an enhanced efficiency of 6.08% has been measured experimentally by using mixed electron transport layer with $CsSnI_3$ absorber [11]. Another recent work shows a highest experimental conversion efficiency of 7.50% for the configuration of $CsSnI_3$ absorber with poly (3-hexylthiophene) as HTL [12]. Very recently, a numerical work on the TiO_2/$CsSnI_3$/Spiro-OMeTAD PSC has evaluated a power conversion efficiency of 20.2% with V_{oc} of 0.97 V [13]. However, these efficiencies are still lower than the other available lead-based PSCs. For a PSC to operate efficiently, the HTL material is a pivotal factor. Insertion of HTL can speed up the hole extraction along the minimization of carrier recombination by blocking the electron flow [14]. In this work, for the first time, we have introduced copper sulfide (CuS) as hole transport material with the $CsSnI_3$ absorber with TiO_2 as ETL. CuS is p-type semiconducting material which has previously been utilized as HTL with other inorganic solar cells [15]. Suitable semiconducting properties of CuS attained from DFT-extraction in the present work [16–18], provide proper band alignment with $CsSnI_3$ to reduce the carrier recombination and enhance the PV performance of the cell.

This work represents the simulation and performance analysis of the PSC with the novel architecture of CuS/$CsSnI_3$/TiO_2/ITO by utilizing the SCAPS-1D program. To achieve the optimized performance, the output parameters are evaluated by varying the thickness, doping concentration, and bulk defect density of the absorber.

2. Methods and Materials

This present work has performed first principle DFT utilizing Cambridge Serial Total Energy Package (CASTEP) open-source package [19] on CuS HTL to evaluate the optical and electrical properties and designed a novel heterojunction lead-free $CsSnI_3$ PSC with arrangement of CuS/$CsSnI_3$/TiO_2/ITO. The designed PSC is investigated numerically using the SCAPS-1D which is solved the Poisson's and continuity equation intending to evaluate one and two-dimension semiconductor cells [20]. In the present study, CuS and TiO_2 are utilized as hole transport layer (HTL) at the back of the absorber and electron transport layer (ETL), respectively. Indium tin oxide (ITO) as transparent conducing oxide (TCO) is used in this numerical investigation. Aluminum (Al) having work function of 4.06 eV [21] and Nickel (Ni) having work function of 5.15 eV [21] are used as metallic electrodes at the front contact and back contact, respectively. Table 1 illustrates the electrical and optical parameters used in this numerical investigation to evaluate the output characteristics of the proposed device. The parameters of all the layers are well agreed with some previous experimental and theoretical works [22–31].

Table 1. Parameters used in this study to investigate the device numerically.

Parameters	CuSCN	CuI	NiO_x	MoO_3	CuS	$CsSnI_3$	TiO_2	ITO
Bandgap, E_g (eV)	3.6	3.1	3.8	3	1.55	1.3	3.2	3.5
Electron affinity, χ (eV)	1.7	2.1	1.46	2.5	3.89	3.8	4.1	4.6
Electron/hole mobility ($cm^2 V^{-1} s^{-1}$)	100/25	100/43.9	12/2.8	25/100	12/9	50/400	0.006	10/10
Thickness (μm)	0.1	0.1	0.1	0.1	0.1	0.6	0.05	0.05
Carrier concentration (cm^{-3})	1×10^{18}	1×10^{18}	1×10^{18}	1×10^{18}	4.7×10^{18}	5×10^{17}	1×10^{18}	1×10^{21}
Reference	[22]	[22]	[23]	[24]	[25]	[26–28]	[29,30]	[31]

3. Result and Discussion

3.1. Structural Properties and Band Structure of CuS

In this study, CASTEP toolkit package [19] is engaged to accomplish the geometry optimization, Elastic constants, band structure, density of states, and optical properties computation. The cut-off kinetic-energy of plane wave is 400 eV with grid parameters (a b c) of 10 10 2 having actual spacing 0.014296 (1/Å) 0.014296 (1/Å) 0.014327 (1/Å). The lowest deviation of 27.1% is calculated using the initial cell volume and final optimized cell volume at cutoff energy 400 eV. The generalized gradient approximation (GGA) for the exchange correlation energy is taken, instead of local density approximation (LDA), due to its excellent band structure calculation. The lattice parameters of CuS are a = b = 3.797 Å, c = 16.441 Å, $\alpha = \beta = 90°$, $\gamma = 120°$ [32]. The geometry optimized crystal structure of unit cell is depicted in Figure 1a. Figure 1b shows the band structure for the optimized CuS structure which is in well concurrence with the density of state. Band structure calculation also shows the band-gap of ~1.6 eV. The band-gap analysis of CuS via DFT calculations with hexagonal structure is almost in the concurrence with the band-gap of the hole transport layer (CuS ~ 1.5 eV).

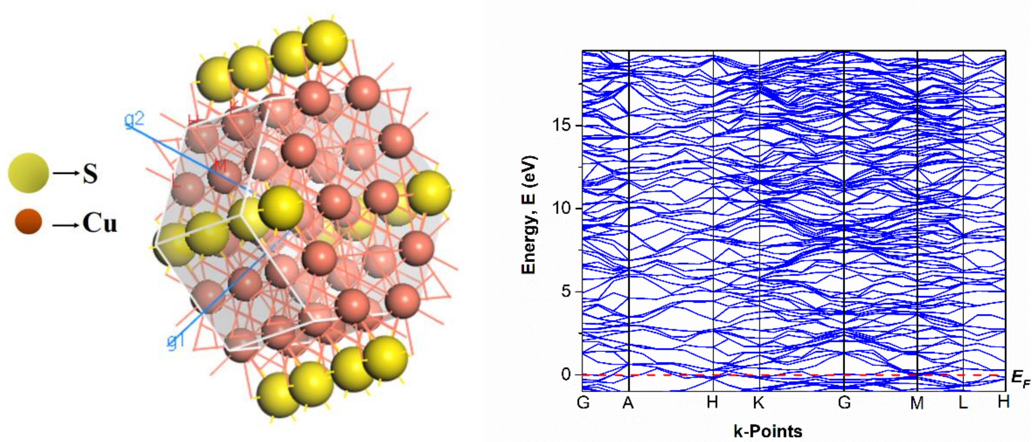

(**a**) (**b**)

Figure 1. (**a**) Crystal structure; (**b**) band structure of CuS.

3.2. Impact of HTLs on Device Performances

To perceive the characteristics of the designed $CsSnI_3$ PSC, numerous HTLs are investigated in this study and the resulted current density-voltage (J-V) characteristics are revealed in Figure 2. This work introduces several HTLs including CuSCN, CuI, CuS, NiOx, and MoO_3 at the back of the $CsSnI_3$ perovskite absorber to improve the proposed device performances by minimizing the losses of charge carrier recombination at the back of the absorber. It is noticed from Figure 2 that lead-free tin based $CsSnI_3$ PSC performances such as open-circuit voltage (V_{oc}), shor circuit current density (J_{sc}), power conversion efficiency (PCE), and fill factor (FF) are improved with inserting the defined HTLs. By inserting HTLs, strong built-in electric field is created at the back of the absorber, thus results in improvement of V_{oc} of the proposed device. Consequently, J_{sc} is also enhanced as ease conduction of charge carrier from absorber to back metal contact and the collection of charge carrier by the electrode. Additionally, introducing HTLs at the back of the absorber may reduce the recombination losses at the back interface and increase the performances of the device. Furthermore, it is important to select the proper HTL among the defined HTLs. The lower negative valance band offset (VBO) is needed to accumulate the holes from the absorber and create the proper band alignment, thus increasing the cell efficiency. Among the different HTLs, CuS has lower VBO than others and gives higher cell outputs which are also illustrated in Figure 2 (inset). Therefore, CuS as HTL is introduced in lead-free $CsSnI_3$ PSC.

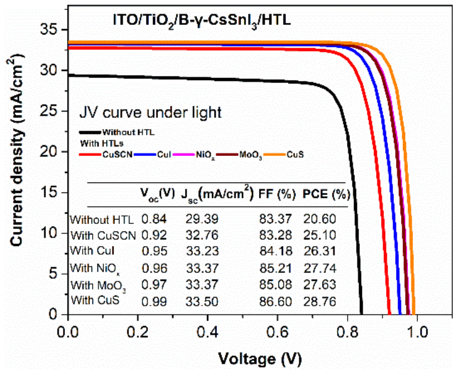

Figure 2. J-V characteristics and solar outputs with different HTLs.

3.3. Effect of Absorber Thickness on Cell Performances

The photon energy is absorbed by the absorber layer. In order to realize the device characteristics, thickness of the $CsSnI_3$ perovskite absorber layer is shifted from 0.1 µm to 1.4 µm as presented in Figure 3a. Thickness of 0.1 µm, 0.05 µm, and 0.05 µm for CuS HTL, TiO_2 ETL, and ITO, respectively, are fixed during the analysis of absorber layer thickness. It is revealed from the figure that V_{oc} is decreased with increasing the absorber layer thickness till 1.2 µm and then it is almost saturated. The degradation of V_{oc} with absorber thickness can be described as the increment of series resistance and recombination rate. On the contrary, J_{sc} is linearly increased upto the absorber thickness of 0.4 µm as the improved generated charge carriers and a comparatively small increment of J_{sc} is observed beyond the thickness of 0.5 µm. The absorption of light is significantly lower when the thickness of the absorber layer is lower, therefore thicker absorber is needed to absorb the sufficient light for enhancing the current density and efficiency. The variation of fill factor (FF) did not changed notably throughout the entire thickness of the absorber. In addition, the PCE is improved upto the absorber thickness of 0.6 µm. Beyond 0.6-µm-thick absorber, less significant enhancement of the PCE is observed. Therefore, absorber thickness is optimized to be 0.6 µm. At the thickness of 0.6 µm, PCE is recorded to be 28.76% including V_{oc} of 0.99 V, J_{sc} of 33.5 mA/cm^2, and FF of 86.6% in the present study.

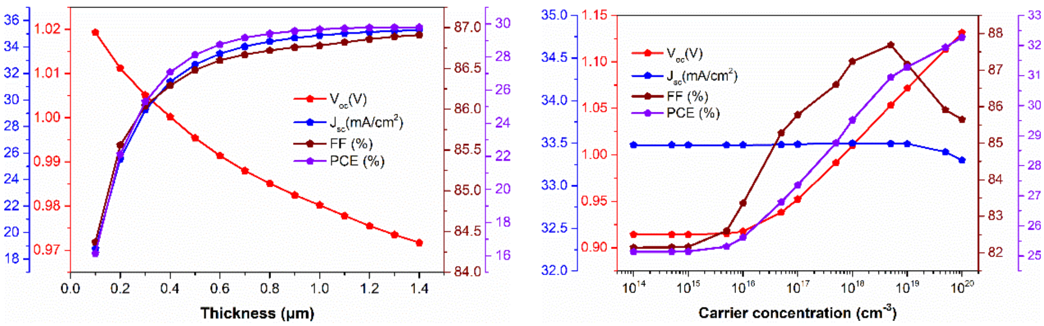

(**a**) (**b**)

Figure 3. Characteristics of CsSnI3 perovskite solar cell with (**a**) absorber layer thickness; (**b**) carrier concentration.

3.4. Effect of Carrier Concentration on Cell Performances

To perceive the output characteristics of the proposed device in accordance with carrier concentration of the absorber, the range from 10^{14} cm^{-3} to 10^{20} cm^{-3} of carrier concentration of the absorber is examined. Figure 3b represents the variation of carrier concentration of the absorber. During the investigation of doping density of absorber, doping density of 10^{19} cm^{-3}, 10^{18} cm^{-3}, and 10^{21} cm^{-3} for CuS HTL, TiO_2 ETL, and ITO, respectively, are fixed. It is noticed from Figure 3b that, device output parameters such as V_{oc}, FF, and

PCE are incremented with boosting the doping density of the absorber. Improvement of carrier concentration in the absorber layer may create enough charge carriers, thereby enhancing the PV performances of the perovskite solar device. The value of PCE > 28.76% and V_{oc} > 0.99 V are measured when the doping density is larger than 5 × 10^{17} cm^{-3}. Conversely, J_{sc} is declined with boosting the absorber carrier concentration as the increment of augur recombination and resistivity of the absorber. At doping density of 5 × 10^{17} cm^{-3}, J_{sc} of 33.5 mA/cm^2 is estimated. This works optimized the doping density of 5 × 10^{17} cm^{-3} considering the overall performances and this optimized value has consistency with the previous experimental works [27].

3.5. Effect of Temperature on Cell Performances

The characteristics and output parameters of solar cells are immensely dependent on temperature. The reduction in energy bandgap of the material allows spare absorption of the photons of small energy which leads to increase the short-circuit current. On the other hand, reduction in the bandgap results in diminishing the open-circuit voltage [33,34]. In the interest of realizing the stability of PSCs, the influence of temperature on device performances is shifted from 283 K to 483 K as depicted in Figure 4. As is noticeable from the figure that, the device output parameters including V_{oc}, PCE, and FF are declined with escalating the conducting temperature. V_{oc} of 1.02 V, PCE of 29.79%, and FF of 88.01% are determined at temperature of 273 K and these values are reduced to 0.75 V, 77.2%, and 19.36% for V_{oc}, PCE, and FF, respectively, at temperature 473 K. The value of J_{sc} is rarely increased with temperature as almost constant as the reverse-saturation current density ameliorates with temperature [34].

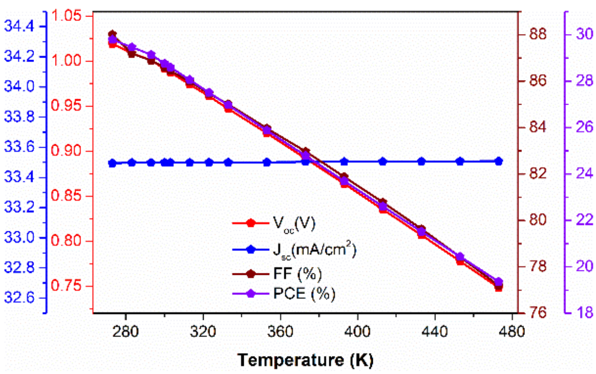

Figure 4. Influence of temperature on the designed perovskite solar cell.

4. Conclusions

This work designs lead-free tin based B-γ-$CsSnI_3$ PSC with the arrangement of CuS/$CsSnI_3$/TiO_2/ITO where the CuS is utilized as HTL, TiO_2 as ETL. Initially, some optical and electrical properties are analyzed for CuS HTL using the first principle density functional theory (DFT). After that, the characteristics of the proposed device structure are assessed numerically by using the SCAPS-1D. The PV performances are evaluated by varying the thickness, carrier concentration of the absorber layer. Herein, numerous HTLs have been realized to adopt the worthy HTL for B-γ-$CsSnI_3$ PSC. The best power conversion efficiency (PCE) of 28.76% containing V_{oc} of 0.99 V, J_{sc} of 33.5 mA/cm^2, and FF of 86.6% has been attained with the optimized thickness of 0.1 μm, 0.6 μm, 0.05 μm, and 0.05 μm for the CuS HTL, absorber, TiO_2 ETL, and ITO, respectively. After providing the overall examination on B-γ-$CsSnI_3$ PSCs, this work has recommend that CuS can be utilized as prominent HTL at the back of the absorber to design and fabricate earth abundant and cost-effective B-γ-$CsSnI_3$ PSC.

Author Contributions: Conceptualization, A.H.; methodology, A.H.; software, A.H.; validation, A.H.; formal analysis, A.H., M.B., S.R. and S.R.A.A.; investigation, A.H.; resources, A.H., S.R. and S.R.A.A.; data curation, A.H.; writing—original draft preparation, A.H. and S.R.; writing—review and editing, M.B. and S.R.A.A.; visualization, A.H., M.B., S.R. and S.R.A.A.; supervision, S.R.A.A. All authors have read and agreed to the published version of the manuscript.

Funding: This research received no external funding.

Institutional Review Board Statement: Not applicable.

Informed Consent Statement: Not applicable.

Data Availability Statement: The data that support the findings of this study are available on request from the corresponding author.

Acknowledgments: The authors also wish to thanks Marc Burgelman and his companions, University of Gent, Belgium for providing the SCAPS simulation package.

Conflicts of Interest: The authors declare no conflict of interest.

References

1. Kim, J.Y.; Lee, J.-W.; Jung, H.S.; Shin, H.; Park, N.-G. High-Efficiency Perovskite Solar Cells. *Chem. Rev.* **2020**, *15*, 7867–7918.
2. Kim, G.-H.; Kim, D.S. Development of perovskite solar cells with >25% conversion efficiency. *Joule* **2021**, *5*, 1033–1035.
3. Su, P.; Liu, Y.; Zhang, J.; Chen, C.; Yang, B.; Zhang, C.; Zhao, X. Pb-Based Perovskite Solar Cells and the Underlying Pollution behind Clean Energy: Dynamic Leaching of Toxic Substances from Discarded Perovskite Solar Cells. *J. Phys. Chem. Lett.* **2020**, *11*, 2812–2817.
4. Schileo, G.; Grancini, G. Lead or no lead? Availability, toxicity, sustainability and environmental impact of lead-free perovskite solar cells. *J. Mater. Chem. C.* **2020**, *9*, 67–76.
5. Kanno, S.; Imamura, Y.; Hada, M. Alternative materials for perovskite solar cells from materials informatics. *Phys. Rev. Mater.* **2019**, *3*, 075403.
6. Giustino, F.; Snaith, H.J. Toward Lead-Free Perovskite Solar Cells. *ACS Energy Lett.* **2016**, *1*, 1233−1240.
7. Wang, N.; Zhou, Y.; Ju, M.-G.; Garces, H.F.; Ding, T.; Pang, S.; Zeng, X.C.; Padture, N.P.; Sun, X.W. Heterojunction-Depleted Lead-Free Perovskite Solar Cells with Coarse-Grained B-γ-CsSnI3 Thin Films. *Adv. Energy Mater.* **2016**, *6*, 1601130.
8. Chung, I.; Song, J.-H.; Im, J.; Androulakis, J.; Malliakas, C.D.; Li, H.; Freeman, A.J.; Kenney, J.T.; Kanatzidis, M.G. $CsSnI_3$: Semiconductor or Metal? High Electrical Conductivity and Strong Near-Infrared Photoluminescence from a Single Material. High Hole Mobility and Phase-Transitions. *J. Am. Chem. Soc.* **2012**, *134*, 8579–8587.
9. Chen, Z.; Wang, J.J.; Ren, Y.; Yu, C.; Shum, K. Schottky solar cells based on $CsSnI_3$ thin-films. *Appl. Phys. Lett.* **2012**, *101*, 093901.
10. Wang, Y.; Tu, J.; Li, T.; Tao, C.; Deng, X.; Li, Z. Convenient Preparation of $CsSnI_3$ Quantum Dots, Excellent Stability, and the Highest Performance of Lead-Free Inorganic Perovskite Solar Cells So Far. *J. Mater. Chem. A*. **2019**, *7*, 7683–7690.
11. Ma, S.; Gu, X.; Kyaw, A.K.; Wang, D.H.; Priya, S.; Ye, T. Fully Inorganic $CsSnI_3$-Based Solar Cells with >6% Efficiency and Enhanced Stability Enabled by Mixed Electron Transport Layer. *ACS Appl. Mater. Interfaces* **2021**, *13*, 1345−1352.
12. Ye, T.; Wang, K.; Hou, Y.; Yang, D.; Smith, N.; Magill, B.; Yoon, J.; Mudiyanselage, R.R.H.H.; Khodaparast, G.A.; Wang, K.; et al. Ambient-Air-Stable Lead-Free $CsSnI_3$ Solar Cells with Greater than 7.5% Efficiency. *J. Am. Chem. Soc.* **2021**, *143*, 4319–4328.
13. Lin, S.; Zhang, B.; Lü, T.-Y.; Zheng, J.-C.; Pan, H.; Chen, H.; Lin, C.; Li, X.; Zhou, J. Inorganic Lead-Free B-γ-$CsSnI_3$ Perovskite Solar Cells Using Diverse Electron-Transporting Materials: A Simulation Study. *ACS Omega* **2021**, *6*, 26689–26698.
14. Głowienka, D.; Zhang, D.; Di Giacomo, F.; Najafi, M.; Veenstra, S.; Szmytkowski, J.; Galagan, Y. Role of Surface Recombination in Perovskite Solar Cells at the Interface of HTL/$CH_3NH_3PbI_3$. *Nano Energy* **2019**, *67*, 104186.
15. Lei, H.; Fang, G.; Cheng, F.; Ke, W.; Qin, P.; Song, Z.; Zheng, Q.; Fan, X.; Huang, H.; Zhao, X. Enhanced efficiency in organic solar cells via in situ fabricated p-type copper sulfide as the hole transporting layer. *Sol. Energy Mater Sol. Cells* **2014**, *128*, 77–84.
16. Sheardy, A.T.; Arvapalli, D.M.; Wei, J. Novel microwave synthesis of near-metallic copper sulfide nanodiscs with size control: Experimental and DFT studies of charge carrier density. *Nanoscale Adv.* **2020**, *2*, 1054–1058.
17. Santos Cruz, J.; Mayén Hernández, S.A.; Paraguay Delgado, F.; Zelaya Angel, O.; Castanedo Pérez, R.; Torres Delgado, G. Optical and Electrical Properties of Thin Films of CuS Nanodisks Ensembles Annealed in a Vacuum and Their Photocatalytic Activity. *Int. J. Photoenergy* **2013**, *2013*, 1–9.
18. Yang, Y.-P.; Zhang, Z.-W.; Shi, Y.-L.; Feng, S.; Wang, W.-Z. Far-infrared conductivity of CuS nanoparticles measured by terahertz time-domain spectroscopy. *Chin. Phys. B* **2010**, *19*, 043302.
19. Clark, S.J.; Segall, M.D.; Pickard, C.J.; Hasnip, P.J.; Probert, M.J.; Refson, K.; Payne, M.C. First principles methods using CASTEP. *Zeitschrift Fur Kristallographie* **2005**, *220*, 567–570.
20. Burgelman, M.; Decock, K.; Niemegeers, A.; Verschraegen, J.; Degrave, S. SCAPS Manual (version: 3.3.07). Department of Electronics and Information Systems, University of Gent, Belgium. Available online: http://scaps.elis.ugent.be (accessed on Date March 2022).
21. Michaelson, H.B. The work function of the elements and its periodicity. *J. Appl. Phys.* **1977**, *48*, 4729–4733.

22. Pitchaiya, S.; Natarajan, M.; Santhanam, A.; Asokan, V.; Yuvapragasam, A.; Madurai Ramakrishnan, V.; EPalanisamy, S.; Sundaram, S.; Velauthapillai, D. A Review on the Classifications of Organic/Inorganic/Carbonaceous Hole Transporting Materials for Perovskite Solar Cell Application. *Arab. J. Chem.* **2020**, *13*, 2526–2557.
23. Kumar, R.R.; Pandey, S.K. Performance evaluation and material parameter perspective of eco-friendly highly efficient CsSnGeI3 perovskite solar cell. *Superlattices Microstruct.* **2019**, *135*, 106273.
24. Li, W.; Li, W.; Feng, Y.; Yang, C. Numerical analysis of the back interface for high efficiency wide band gap chalcopyrite solar cells. *Sol. Energy* **2019**, *180*, 207–215.
25. PVEducation. Available online: https://www.pveducation.org/pvcdrom/materials/cus (accessed on 3 May 2022).
26. Chung, I.; Lee, B.; He, J.; Chang, R.P.H.; Kanatzidis, M.G. All-solid-state dye-sensitized solar cells with high efficiency. *Nature* **2012**, *485*, 486–489.
27. Wu, B.; Zhou, Y.; Xing, G.; Xu, Q.; Garces, H.F.; Solanki, A.; Goh, T.W.; Padture, N.P.; Sum, T.C. Long Minority-Carrier Diffusion Length and Low Surface-Recombination Velocity in Inorganic Lead-Free $CsSnI_3$ Perovskite Crystal for Solar Cells. *Adv. Funct. Mater.* **2017**, *27*, 1604818.
28. Chung, I.; Song, J.H.; Im, J.; Androulakis, J.; Malliakas, C.D.; Li, H.; Freeman, A.J.; Kenney, J.T.; Kanatzidis, M.G. $CsSnI_3$: Semiconductor or metal? High electrical conductivity and strong near-infrared photoluminescence from a single material. High hole mobility and phase-transitions. *J. Am. Chem. Soc.* **2012**, *134*, 8579–8587.
29. Jung, H.S.; Park, N.G. Perovskite solar cells: From materials to devices. *Small* **2015**, *11*, 10–25.
30. van de Krol, R.; Goossens, A.; Schoonman, J. Mott-Schottky analysis of nanometer-scale thin-film anatase TiO_2. *J. Electrochem. Soc.* **1997**, *144*, 1723–1727.
31. Rahman, M.A. Enhancing the photovoltaic performance of Cd-free Cu_2ZnSnS_4 heterojunction solar cells using SnS HTL and TiO_2 ETL. *Sol. Energy* **2021**, *215*, 64–76.
32. Materials Project. Available online: https://materialsproject.org/materials/mp-504/ (accessed on 3 May 2022).
33. Varshni, Y.P. Temperature dependence of the energy gap in semiconductors. *Physica* **1967**, *34*, 149–154.
34. Singh, P.; Ravindra, N.M. Temperature dependence of solar cell performance-an analysis. *Sol. Energy Mater. Sol. Cells* **2012**, *101*, 36–45.